PAPER *Special Issue on Machine Vision and Applications*

Estimation of the Visibility Distance by Stereovision: a Generic Approach

Nicolas HAUTIERE[†a)], Raphaël LABAYRADE[†], *and* Didier AUBERT[†], *Nonmembers*

SUMMARY   An atmospheric visibility measurement system capable of quantifying the most common operating range of on-board exteroceptive sensors is a key parameter in the creation of driving assistance systems. This information is then utilized to adapt sensor operations and processing or to alert the driver that the onboard assistance system is momentarily inoperative. Moreover, a system capable of either detecting the presence of fog or estimating visibility distances constitutes in itself a driving aid. In this paper, we first present a review of different optical sensors likely to measure the visibility distance. We then present our stereovision based technique to estimate what we call the "mobilized visibility distance". This is the distance to the most distant object on the road surface having a contrast above 5%. In fact, this definition is very close to the definition of the meteorological visibility distance proposed by the International Commission on Illumination (CIE). The method combines the computation of both a depth map of the vehicle environment using the "v-disparity" approach and of local contrasts above 5%. Both methods are described separately. Then, their combination is detailed. A qualitative evaluation is done using different video sequences. Finally, a static quantitative evaluation is also performed thanks to reference targets installed on a dedicated test site.
key words: *meteorological visibility, fog, contrast, stereovision, sensor, driving assistance, intelligent transportation systems.*

1. Introduction

The visual perception of the environment is in the heart of the driving process (about 90% of perceptual information). Consequently, a loss of visibility due to adverse meteorological conditions is typically a source of accidents. Thus, detecting such situations can contribute to the improvement of the road safety. First of all, one can automate tasks such as turning on the lights or alerting the driver that his speed is not adapted to the visibility conditions. Indeed, during foggy weather, humans tend to overestimate visibility distances [1], which can lead to excessive driving speeds. Then, an atmospheric visibility measurement system may be also capable of quantifying the most common operating range of onboard exteroceptive sensors (cameras, laser, radar). Thus, driving assistances relying on the outputs of theses devices can be adapted, and eventually stopped according to the visibility conditions.

The objective of this paper is to build a generic method able to measure the visibility distance. We first define the notion of visibility distance. Then, we review different optical sensors likely to be onboard a moving car and justify the choice of a camera. Existing solutions using a camera are summarized. The limits of each one are given, which allows us to build and to validate a new approach in the rest of the paper.

2. Optical Measurement of the Meteorological Visibility

In this section, we review different sensors that could be used to estimate the meteorological visibility. Let us begin by giving a look at Fig. 1 given in [2]. This curve depicts the atmospheric attenuation due to dense fog (V=50 m) according to the frequency of the signal. We can state that automotive RADARS (24 GHz or 77 GHz) are not adapted to estimate the attenuation of the visual signal due to the presence of fog, contrary to optical sensors working in the infrared or visible domain. Thus, in the following, we first deal with the notion of meteorological visibility. The relevance of different optical sensors to estimate the meteorological visibility onboard a moving vehicle is then studied.
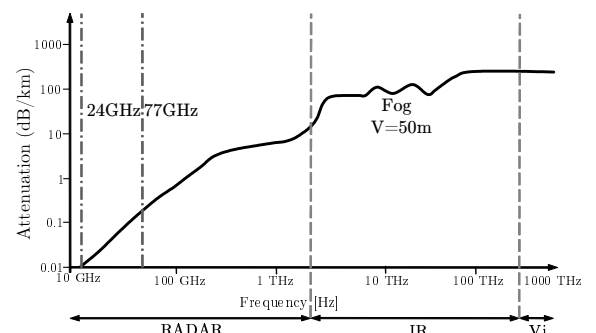
Fig. 1   Curve, partially issued from [2], depicting the atmospheric attenuation due to dense fog (V=50 m) according to the frequency of the signal.
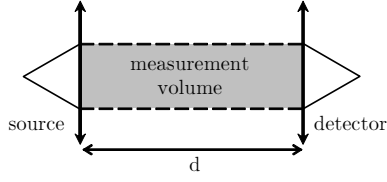
2.1 Meteorological Visibility

Fog is thick cloud of microscopic water droplets suspended at ground level. When light propagating in fog

Fig. 2 The operating principle of a transmissometer is to measure the average transmissivity of the atmosphere along a given path.

encounters a droplet, the luminous flux is scattered in all directions. For visible light, the absorption can be negligible. The amount of energy that is lost along the way is described by the lineic optical density k (m^{-1}), known as the extinction coefficient. It depends on the droplet size distribution and the concentration. The proportion of energy transmitted between two points in fog is known as the transmissivity T. According to Beer-Lambert's Law, it decreases exponentially with distance d:

$$T = e^{-kd} \tag{1}$$

The effect of light scattering in the presence of fog is to modify this information by an overall reduction of contrasts as a function of distance. This effect is generally described by the meteorological visibility V_{met}, defined as the greatest distance at which a black object can be recognized by day against the horizon sky [3]. Using (1) with a contrast threshold of 5% yields the following approximate relation between V_{met} and the extinction coefficient k:

$$V_{met} = -\frac{1}{k}\ln(0.05) \simeq \frac{3}{k} \tag{2}$$

Details about fog effects on road vision can be found in [4].

2.2 Road Visibilitymeters

This lexicographical term serves to designate two main types of instruments for both detecting fog and measuring the extinction coefficient k; they are transmissometers and scatterometers [5].

2.2.1 Transmissometers

The basic principle behind this category of instrument consists of measuring average transmissivity of the atmosphere along a given path (see Fig. 2). Transmissometers are composed of both a projector comprising a source emitting a luminous flux ϕ_0 within the visible domain and a receiver set located at an invariable distance d that measures the luminous flux ϕ received.

By using Beer-Lambert's Law, the extinction coefficient of the fog k, used for calculating the visibility distance (2), is given by:
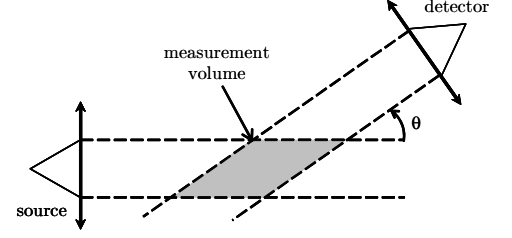
Fig. 3 The operating principle of a scatterometer is to measure the light diffused in a well-defined solid angle.

$$k = \frac{1}{d}\ln\left(\frac{\phi}{\phi_0}\right) \tag{3}$$

The transmissometers are reliable. Their sensitivity is related to the length of the measurement base d. This length, which extends over several meters or even several tens of meters, provides these devices with a high level of accuracy, given the lack of homogeneity often encountered in fog. Transmissometers however are costly to implement and the optical block alignment frequently proves to be a complex procedure.

2.2.2 Scatterometers

Some of these devices were developed for road applications, primarily for conducting measurements under conditions of thick fog. They enable quantifying the light diffused within a sufficiently wide and well-defined solid angle. In order to carry out such measurements, a light beam is concentrated on a small volume of air (see Fig. 3). The proportion of light being diffused toward the receiver would then be:

$$I = AI_0Vf(\theta)e^{-kd} \tag{4}$$

with I the intensity diffused in the direction of the receiver, A a constant dependent on power and source optics, I_0 the source intensity, V the diffusing volume, $f(\theta)$ the value of the diffusion function in the θ direction, k the extinction coefficient and d the length of the optical path between emitter and receiver.

Generally speaking, the optical path d is small and the transmission factor e^{-kd} is assimilated to 1 and $f(\theta)$ is proportional to k, with (4) thereby becoming:

$$I = A'I_0k, \text{ then } k = \frac{1}{A'}\frac{I}{I_0} \tag{5}$$

where A' designates a constant that depends on device characteristics.

We can state that a scatterometer, to its advantage, is significantly less expensive than a transmissometer and that no optical block alignment is required. On the other hand, the small size of the diffusing volume makes measurements highly sensitive to non-homogeneities in the fog. Furthermore, the sensor accuracy decreases with the meteorological visibility
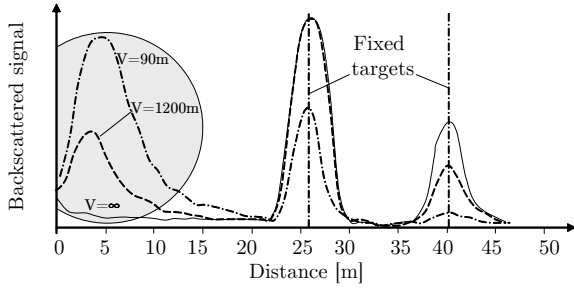
Fig. 4 Backscattered signal by a LIDAR in the presence of artificial fog [7]. The diagram also shows the detection of two fixed targets.

and is not acceptable for visibilities below 50m.

Consequently, neither a transmissometer or a scatterometer can be placed onboard a moving vehicle. Indeed, the measurement path is too short and the aligment of optical blocks is difficult for a transmissometer. A scatterometer would be too sensitive to the turbulence caused by the motion of the vehicle.

2.3 LIDAR

In the literature, one can find some articles on the use of a LIDAR in the presence of fog, which can be classified into two categories. The first application consists in detecting objects located further than the meteorological visibility distance by using a laser beam whose power is greater than the atmospheric attenuation. This is the case of Pirroda [6]. We are not concerned by this type of application.

In the second application, LIDARS are used to estimate the visibility conditions by measuring the signal backscattered by fog droplets (Fig. 4) and then to adjust the level of lights of a moving car according to the meteorological conditions [7], [8]. However, it has also been shown [9] that the power of the LIDAR must be adapted according to the extinction coefficient of the atmosphere k.

2.4 Camera

If a camera is used, there is no need to align the optical units as it is the case with the transmissometer, and an image is obtained which is representative of the environment, unlike with a scatterometer. Finally, in the case of a classical camera, the spectra taken into account is in the visible domain. Consequently, its image is degraded by the presence of fog. Most approaches make use of a fixed camera placed on the roadway which simplifies the task as a reference image is always available [10], [11].

Systems that entail use of an onboard camera are encountered less frequently. Pomerleau [12] estimates visibility by means of measuring a contrast attenuation per meter on the road markings at various distances in

front of the vehicle. However, this approach based on the RALPH System [13] only indicates a relative visibility distance and requires the detection of road markings to run. Yahiaoui [14] estimates the quality of images by comparing the MTF of the current image with the contrast sensitivity function of Mannos [15]. However, it only returns a potential visibility distance. So, these methods estimate what could be the maximum visibility distance in the scene. In our approach, we expect to estimate the real current existing visibility distance, which better characterizes the vehicle environment.

Thus, in [16], we succeed to instantiate Koschmieder's model and then to estimate the meteorological visibility distance. This method, when its operation assumptions are met, allows us to obtain good results by daytime foggy weather. An extension of the method has been proposed in [17]. In order to cover more meteorological situations than solely foggy weather, we propose in this paper a generic method to estimate what we call the "mobilized visibility distance" (section 3). In this aim, we estimate the distance to the most distant object on the road surface having a contrast above 5%. Thus, this method is very close to the definition of the CIE.

The method is broken up into three parts. The first one presents a method to compute a depth map of the environment of the vehicle (section 4). The second part presents a method to extract picture elements whose contrast is above 5% (section 5). Finally, thanks to the combination of both previous techniques, the mobilized visibility distance can be obtained (section 6). The method is evaluated thanks to video sequences and static reference measurements (section 7).

3. Mobilized and Mobilizable Distances of Visibility

On Fig. 5, we represent a simplified road. We can see from the Fig. 5a that the most distant visible object is the extremity of the furthest road marking. It could be the roadside, a shadow... However, the extremity location depends on the vehicle position. We call this distance to the most distant visible object, which depends on the road scene, the mobilized visibility distance V_{mob}. This distance has to be compared to the mobilizable visibility distance V_{max}. This is the maximum distance at which an object on the road surface would be visible.

Koschmieder's Law [18] gives us the theoretical variations of both the road luminance and the luminance of an object on its surface. We denote $\tilde{\varepsilon}$ the contrast threshold below which the object on the road surface is considered as being not visible. Thus, the value of V_{max} according to the meteorological visibility distance (2) is therefore:
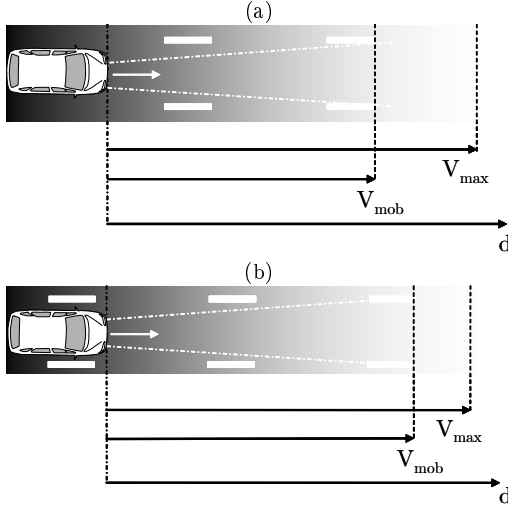
Fig. 5 Examples of mobilized V_{mob} and mobilizable V_{max} distances of visibility.

$$V_{max} = -\frac{V_{met}}{3} \ln \left(\frac{\tilde{\varepsilon}}{1 + \tilde{\varepsilon}} \right) \qquad (6)$$

We obtain easily the value $\tilde{\varepsilon}$ so that $V_{max} = V_{met}$:

$$\tilde{\varepsilon} = \frac{1}{e^3 - 1} \approx 5\% \qquad (7)$$

Consequently, by choosing a threshold of 5%, the mobilizable visibility distance is very close to the meteorological visibility distance (2). These definitions lead to the following relationship:

$$V_{mob} \leq V_{max} \approx V_{met} \qquad (8)$$

## 4. Computation of a Depth Map of the Environment by Stereovision

In this section, we present our stereoscopic sensor. Then, we describe briefly our technique to obtain a depth map of the environment using the "v-disparity" approach, which computes robustly the disparity on the road surface (not necessarily plane). The different stages of computation of this depth map are detailed.

4.1 Modeling of the Stereo Sensor

The two image planes of the stereo sensor are supposed to belong to the same plane and are at the same height above the road (see Fig. 6). This camera geometry means that the epipolar lines are parallel.

4.2 The Image of a Plane in the "v-disparity" Image

In this study, we segment the environment into planes which are horizontal, vertical or oblique with respect to the plane of the stereoscopic sensor. In a cross-section
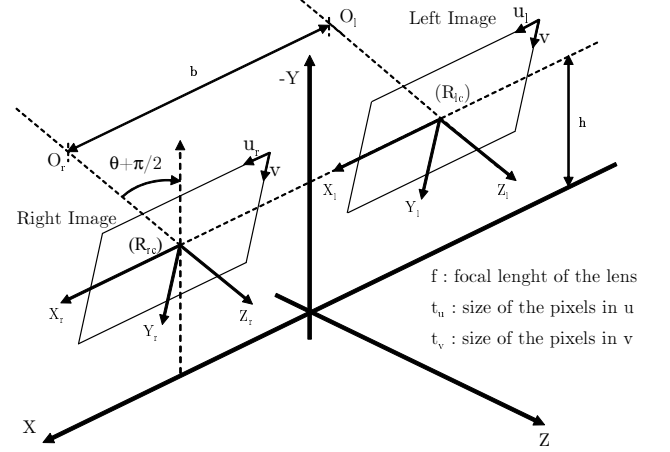
Fig. 6 The stereo sensor and the coordinate systems used.

of the scene in the optical axis of the camera, the projection of any of these planes is a straight line. In the rest of this paper, we use a specific image representation, in which the detection of straight lines is equivalent to the detection of planes in the scene. Indeed, we represent the v coordinate of a pixel towards the disparity Δ and detect straight lines and curves in this 2-D image. The mathematical details are given in [19].

4.3 "V-disparity" Image Construction and 3-D Surface Extraction

To compute a disparity map I_Δ, the primitives used are horizontal local maxima of the gradient. The matching process is based on normalized correlation around the local maxima. It is quite simple and fast. Once I_Δ has been computed, the "v-disparity" image $I_{v\Delta}$ is built by accumulating the pixels of same disparity in I_Δ along the $\vec{v}$ axis. Then straight lines are detected in $I_{v\Delta}$ thanks to a Hough transform. This leads to extract global surfaces, which correspond either to the road surface, or to obstacles. Details of this method are given in [19]. The accuracy of the method is presented in [20].

4.4 Disparity Map Improvement

In order to quickly compute the "v-disparity" image, a sparse and rough disparity map has been built. This disparity map may contain numerous false matches, which prevents us to use it as a depth map of the environment. Thanks to the global surfaces extracted from the "v-disparity" image, false matches can be removed. In this aim, we check whether a pixel of the disparity map belongs to any global surface extracted using the same matching process. Thus, if the pixel belongs to the road surface, the disparity value is mapped to the pixel. Else, if the pixel belongs to another global surface, the white value is mapped to the pixel.

Thus, the idea is to improve the disparity map from
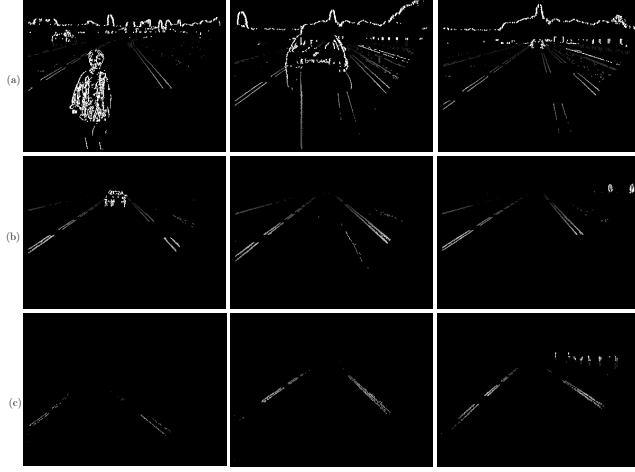
Fig. 7 Examples of disparity map of the vehicle environment (a) under sunny weather, (b) under daily foggy weather, (c) under night foggy weather. White pixels are considered as obstacles points. The gray level of other pixels is proportional to their disparity.

Fig. 8 Examples of computation of contrasts above 5%, (a) under sunny weather, (b) under daily foggy weather, (c) under night foggy weather.

the geometry knowledge about the scene obtained from the rough disparity map. Details of this process can be found in [21]. Finally, this enhanced disparity map can be used as a depth map of the vehicle environment.

5. Computation of Contrasts above 5%

5.1 Measuring the Local Contrast with Köhler's Binarization Technique

Köhler's technique [22] used to binarize images finds the threshold which maximizes the contrast between two parts of the image. Let f be a gray level image. Let consider a neighbourhood N in this image. A couple of pixels $(x, x_1) \in N$ is said to be separated by the threshold s if two conditions are met. First, $x_1 \in V_4(x)$ (4-connexity neighbourhood of pixel x). Secondly, the condition (9) is respected:

$$\min(f(x), f(x_1)) \leq s < \max(f(x), f(x_1)) \quad (9)$$

Let $F(s)$ be the set of all couples $(x, x_1) \in N$ separated by s. With these definitions, for every value of s belonging to [0,255], $F(s)$ is built. For every couple belonging to $F(s)$, the local contrast $C_{x,x_1}(s)$ is computed.
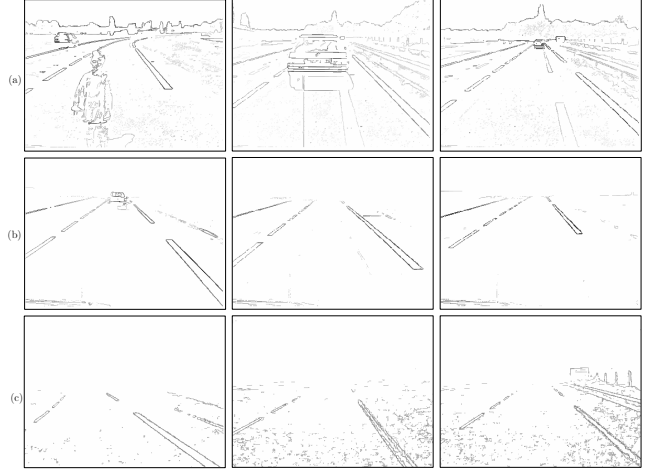
$$C_{x,x_1}(s) = \min\left(|s - f(x)|, |s - f(x_1)|\right) \quad (10)$$

The mean contrast (11) associated to $F(s)$ is then performed:

$$C(s) = \frac{1}{\#F(s)} \sum_{(x,x_1) \in F(s)} C_{x,x_1}(s) \quad (11)$$

where $\#F(s)$ designates the cardinal of the set $F(s)$. The best threshold s_0 verifies the following condition:

$$C(s_0) = \max_{s \in [0,255]} C(s) \quad (12)$$

s_0 is the threshold which has the best mean contrast along the associated border $F(s_0)$. Instead of using this method to binarize images, we use it to measure the contrast locally.

5.2 Adaptation to the Logarithmic Contrast

The previous method is suitable for different definitions of local contrast. To use another local contrast definition, it is enough to use the desired definition in the place of (10). In our case, we have chosen to estimate Weber's contrast [23] or logarithmic contrast [24], so as to be compatible with the definition of the meteorological visibility distance proposed by the CIE (2). So, (10) becomes :

$$C_{x,x_1}(s) = \min\left[\frac{|s - f(x)|}{\max(s, f(x))}, \frac{|s - f(x_1)|}{\max(s, f(x_1))}\right] \quad (13)$$

Thus, using (13) to compute (12), if $2C(s_0) \geq 5\%$, the set of pixels $\in N$ having a contrast above 5 % is $F(s_0)$.

5.3 Adaptation of the Technique to our Needs

Our technique, inspired from Köhler, is robust to noise. The computational cost of the technique is high. However, a direct implementation of the technique takes 14 s to be performed on a whole image of resolution 380×289 on a Pentium IV 2.4 GHz. By reducing the thresholds number to compute (11) and precalculating the MIN-MAX images (lookup tables to accelerate the computation of (9)), the computing time is inferior to 1s. By vectorizing this optimized algorithm, the computational cost is finally about 350ms on a whole image. Samples of contrast computation are given on Fig. 8.

6. Estimation of the Mobilized Visibility Distance

In section 4, we described the computation of a depth map of the vehicle environment, where the disparity on the road surface is computed and vertical objects are detected. In section 5, we presented a method to compute the local contrast above 5%. To estimate the visibility distance, we have to combine both to estimate the most distant picture element belonging to the road surface having a contrast above 5%.

6.1 Direct Disparity-Contrast Combination

The first approach is to replace the computation of the horizontal local maxima of the gradient by the horizontal contrasts above 5% to compute the disparity map (cf. section 4.3). Horizontal contrast is obtained by replacing $V_4(x)$ by the left and right connexity neighbourhood of pixel x, in order to compute (9). Thus, the visibility distance is the distance of the pixel having the smallest disparity. This approach is simple. Its main advantage is to replace the gradient threshold, which is empirically chosen, by the contrast threshold of 5%. Unfortunately, it is too much time consuming for our real-time application.

6.2 Fast Disparity-Contrast Cooperation

The contrast computation locates precisely the edges, but is quite expensive in term of computing times. Conversely, the gradients computation goes fast but spreads on the edges. Consequently, using the horizontal gradients, the "v-disparity" image is denser and faster to compute. The 3-D surface extraction is also faster and more reliable. However, we must ensure that the gradient threshold is small enough, so as to take most picture elements having a contrast above 5% into account, but high enough so as to not take noise into account. The noise measured on the cameras currently in use is gaussian with a standard deviation σ of 1 to 2 gray levels. The gradient threshold to consider is then 3σ, that is to say 6.

It is possible to draw advantage from the two techniques while decreasing the computing time compared to the only use of horizontal contrasts. The method consists in computing the improved disparity map using the horizontal gradients higher than 6 and to scan it. Because most distant objects on the road surface are on the horizon line, the scanning starts from the horizon line (intersection of vanishing lines obtained thanks to the "v-disparity" image [19]). Within each neighbourhood N belonging to the road surface where a point of disparity is known the contrast is computed. The process stops when a contrast above 5% is met. The visibility distance is then the depth of the picture element
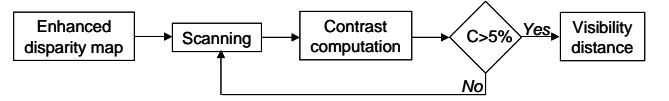

Fig. 9   Algorithm overview

with a contrast above 5%. This process is summarized on Fig. 9.

7. Experimental Evaluation

7.1 Qualitative Evaluation

7.1.1 Hardware settings

The whole process for building the depth map of the vehicle environment and computing the mobilized visibility distance is frame rate performed (25 Hz) with a current-day PC (Intel bi-Xeon 2.4 GHz). Images are grabbed using a Matrox Meteor II graphic card. The focal length is 8.5 mm and image size is 380×289. The program runs on the RT-Maps platform [25]. It is compiled with the Intel C++ Compiler 8.0 and runs onboard the prototype vehicle presented on the Fig. 10.

7.1.2 Results

On Fig. 7, results of the disparity map computation are presented. On Fig. 7a, the pedestrian, the car and points beyond horizon line are considered as obstacles points. The depth of the points on the road surface is computed. In the same way, on Fig. 7b, the car is considered as an obstacle.

On Fig. 8, results of local contrast computation on the whole images are represented. In fact, as explained in section 6, the contrast will not be computed on the whole image to save computing time. On Fig. 11, the final result is displayed.

Finally on Fig. 12, the curves of measured visibility distances are plotted for three video sequences of 1000 images each. Under sunny weather, the maximum resolution of the stereoscopic sensor is reached. Under foggy weather, the measures are quite stable which let

Fig. 10   VIPER: a prototype vehicle equipped with exteroceptive sensors (3 cameras, 1 RADAR, 4 LIDARS), proprioceptive sensors (INS, accelerometers), actuators (brakes, steering wheel, gas pedal) and GPS RTK.
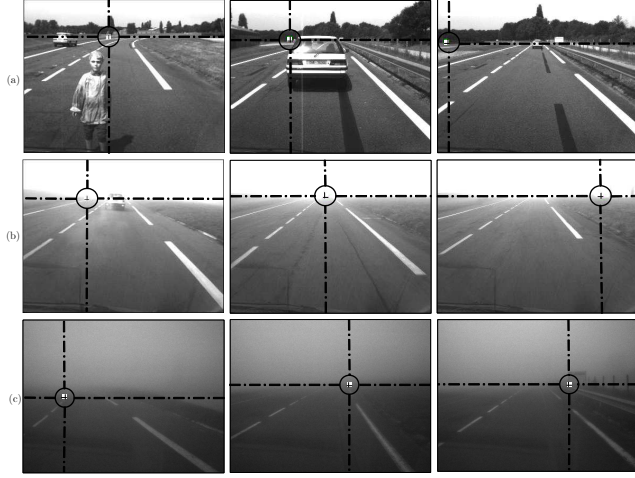
Fig. 11 Final result: the most distant window having a contrast above 5 %, on which a point of disparity is known, is painted white. The disparity point is represented with a black cross inside the white window. (a) sunny weather ($V_{mob} \approx 260$ m), (b) daily foggy weather ($V_{mob} \approx 75$ m), (c) night foggy weather ($V_{mob} \approx 40$ m).

us think that the method is efficient in poor visibility conditions. The visibility distance measurement for a video sequence under dense fog before night-fall is given as well.

7.2 Quantitative Evaluation

7.2.1 Equipment of a Dedicated Site

So far, our methods have only been evaluated qualitatively, through a subjective analysis of the mean and standard deviation of the measures in the cases of different rides in adverse visibility conditions. Quantitative assessment has not been endeavored yet, due to the lack of a reference visibility sensor. We have equipped our test track in Versailles (France) with six large specific signs, located between 35m and 200m from the cameras onboard the stationed vehicle. The idea is to take pictures of these targets in adverse visibility conditions and to estimate the extinction coefficient of the atmosphere k based on the attenuation of their contrast (cf. Fig. 13). Thus, by comparing two targets the value of k is:

$$k = -\frac{1}{d_2 - d_1} \ln \left[\frac{L_w(d_2) - L_b(d_2)}{L_w(d_1) - L_b(d_1)} \right] \qquad (14)$$

where L_b (respectively L_w) denote the luminance of the black (white) part of a target, d_1 the distance to a target, d_2 the distance to another target. From (14) and (2), the visibility distance is then deduced.

7.2.2 Results

The static measurement, which uses the reference tar-
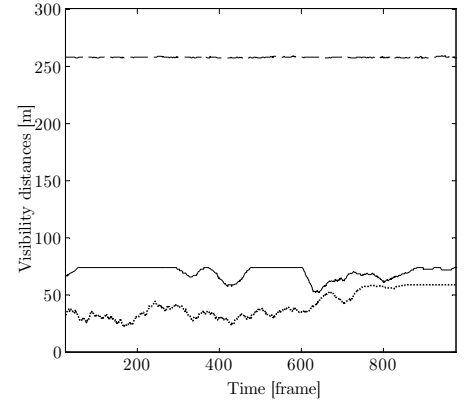
Fig. 12 Curves of measured mobilized visibility distances (– –) under sunny weather, (—) under foggy weather, (...) under dense fog before night-fall.

gets, can then be compared to the results of our onboard dynamic technique, which requires no reference. During last winter, some pictures of the site have been taken under different meteorological conditions. On the whole, ten scenarios have been considered. On Fig. 14, for each scenario, the estimation of the mobilized visibility distance V_{mob} is plotted versus the meteorological visibility distance V_{met} obtained thanks to the reference targets. The straight line $y = x$ (that is to say $V_{mob} = V_{met}$) is also plotted, which allows to say that (8) is verified. However, the correlation score between both measurements is not very good (81%). That is why the correlation line (bold line) does not fit very well. This is absolutely normal, because the mobilized visibility distance directly depends on the objects really present in the scene. Thus, on Fig. 14, one can remark two plateaus (100m and 130m) corresponding to objects in the scene (actually, a parking and a track).

8. Conclusion

In this paper, we presented a generic method based on stereovision to estimate the mobilized visibility distance, which is the distance of the most distant picture element on the road surface having a contrast above 5%. This method is close to the meteorological visibility distance. We use the "v-disparity" stereovision approach

Fig. 13 Picture of the site equipped with reference targets in foggy weather. Weber's contrast between the two parts of the targets is given near each one.
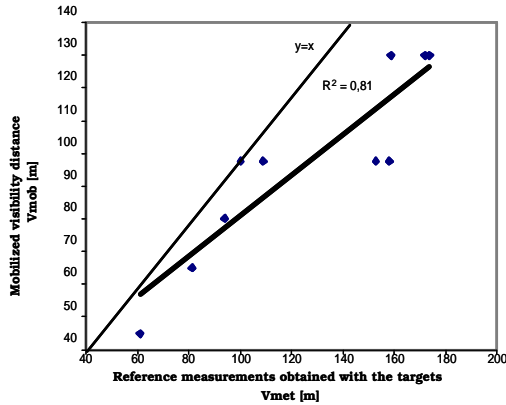
Fig. 14 Points: estimation of the mobilized visibility distance V_{mob} versus the meteorological visibility distance V_{met} obtained thanks to the reference targets. Bold line: correlation line of the points. $y = x$ line: line where $V_{mob} = V_{met}$.

to build a depth map of vehicle environment. We combine this map with the computation of local contrasts by means of a technique inspired by Köhler. The whole process is real-time performed. This technique, which has been recently patented, has very few assumptions. Consequently, it is operative under every meteorological conditions. First of all, experimental validation was conducted thanks to different video sequences by sunny and foggy weather. Then, static tests were made using different pictures grabbed under various visibility conditions on a site, which was equipped with targets.

Acknowledgments

References

[1] V. Cavallo, M. Colomb, and J. Doré, "Distance perception of vehicle rear lights in fog," Human Factors, vol.43, pp.442–451, 2001.

[2] P. Bhartia and I. Bahl, Millemeter Wave Engineering and Applications, John Wiley and Sons, 1984.

[3] International Lighting Vocabulary, Commission Internationale de l'Éclairage, 1987.

[4] E. Dumont and V. Cavallo, "Extended photometric model of fog effects on road vision," Transportation Research Records, no.1862, pp.77–81, 2004.

[5] LCPC, ed., bulletin des laboratoires des Ponts et Chaussées, Février 1993.

[6] L. Pirroda, "Enhancing visibility through fog," Optics and Laser Technology, vol.29, no.6, pp.293–299, 1997.

[7] C. Boehlau, "Optical sensors for AFS - supplement and alternative to GPS," PAL 2001 Symposium, 2001.

[8] F. Rosenstein, "Intelligent rear light - constant perceptibility of light signals under all weather conditions," ISAL 2005, pp.403–414, September 2005.

[9] M. Colomb, "The main results of a european research project: "improvement of transport safety by control of fog production in a chamber" ("FOG")," International Conference on Fog, Fog Collection and Dew, October 2004.

[10] C. Bush and E. Debes, "Wavelet transform for analyzing fog visibility," IEEE Intelligent Systems, vol.13, no.6, pp.66–71, November/December 1998.

[11] T.M. Kwon, "Atmospheric visibility measurements using video cameras: Relative visibility," tech. rep., University of Minnesota Duluth, July 2004.

[12] D. Pomerleau, "Visibility estimation from a moving vehicle using the ralph vision system," IEEE Conference on Intelligent Transportation Systems, November 1997.

[13] D. Pomerleau, "RALPH: Rapidly adapting lateral position handler," IEEE Symposium on Intelligent Vehicles, September 1995.

[14] G. Yahiaoui and P. Da Silva Dias, "In board visibility evaluation for car safety applications: a human vision modelling based approach," ITS World Congress, November 2003.

[15] J. Mannos and D. Sakrison, "The effects of visual fidelity criterion on the encoding of images," IEEE Transactions on Information Theory, vol.IT-20, no.4, pp.525–536, 1974.

[16] N. Hautière and D. Aubert, "Driving assistance: automatic fog detection and measure of the visibility distance," ITS World Congress, November 2003.

[17] N. Hautière and D. Aubert, "Fog detection through use of a CCD onboard camera," VISION 2004, September 2004.

[18] W. Middleton, Vision through the atmosphere, University of Toronto Press, 1952.

[19] R. Labayrade, D. Aubert, and J.P. Tarel, "Real time obstacle detection in stereovision on non flat road geometry through v-disparity representation," IEEE Intelligent Vehicle Symposium, 2002.

[20] R. Labayrade and D. Aubert, "Robust and fast stereovision based road obstacles detection for driving safety assistance," IEICE Transactions on Information and Systems, vol.E87-D, no.1, pp.80–88, January 2004.

[21] R. Labayrade and D. Aubert, "In-vehicle obstacles detection and characterization by stereovision," IEEE ICVS, November 2003.

[22] R. Köhler, "A segmentation system based on thresholding," Graphical Models and Image Processing, vol.15, pp.319–338, 1981.

[23] T. Cornsweet, Visual perception, Academic Press, 1970.

[24] M. Jourlin and J.C. Pinoli, "Logarithmic image processing," Advances In Imaging and Electron Physics, vol.115, pp.129–196, 2001.

[25] F. Nashashibi, B. Steux, P. Coulombeau, and C. Laurgeau, "Rt-maps a framework for prototyping automotive multi-sensor applications," IEEE Intelligent Vehicles Symposium, October 2000.

[26] PREDIT, "ARCOS: Research action for secure driving." http://www.arcos2004.com, 2001–2004.

[27] N. Hautière, R. Labayrade, and D. Aubert, "Dispositif de mesure de distance de visibilité." Brevet français No. 0411061 soumis par LCPC/INRETS, octobre 2004.